ACDiT: Interpolating Autoregressive Conditional Modeling and Diffusion Transformer

Anonymous authors
Paper under double-blind review

Abstract

Autoregressive and diffusion models have achieved remarkable progress in language models and visual generation, respectively. We present ACDiT, a novel **A**utoregressive blockwise **C**onditional **Di**ffusion **T**ransformer, that innovatively combines autoregressive and diffusion paradigms. By introducing a block-wise autoregressive unit, ACDiT offers a flexible interpolation between token-wise autoregression and full-sequence diffusion, bypassing the limitations of discrete tokenization. The generation of each block is formulated as a conditional diffusion process, conditioned on prior blocks. ACDiT is easy to implement, as simple as applying a specially designed Skip-Causal Attention Mask (SCAM) on the standard diffusion transformer during training. During inference, the process iterates between diffusion denoising and autoregressive decoding that can make full use of KV-Cache. We validate the effectiveness of ACDiT on image, video, and text generation and show that ACDiT performs best among all autoregressive baselines on similar model scales on visual generation tasks. We also demonstrate that benefiting from autoregressive modeling, pretrained ACDiT can be transferred to visual understanding tasks despite being trained with the generative objective. The analysis of the trade-off between autoregressive and diffusion demonstrates the potential of ACDiT to be used in long-horizon visual generation tasks. We hope that ACDiT offers a novel perspective on visual autoregressive generation and sheds light on new avenues for unified models.

1 Introduction

The concept of predicting the future has been a fundamental principle of artificial intelligence, ranging from the next token prediction objective of autoregressive language modeling (Radford et al., 2019; Brown, 2020; Achiam et al., 2023) to predicting the next action in Reinforcement Learning (Mnih, 2013; Schulman et al., 2017; Chen et al., 2021; Reed et al., 2022). The recent renaissance of the world model also builds upon forming an internal state that both predicts and is shaped by the prediction of the future (Ha & Schmidhuber, 2018). The success of Large Language Models (LLMs) (Touvron et al., 2023a;b; Brown, 2020; Achiam et al., 2023; Jiang et al., 2023; Bai et al., 2023; Yang et al., 2024) exemplifies the power of such philosophy, demonstrating that complex abilities can arise from this simple objective.

However, the multimodal aspects of information beyond language have yet to fully capitalize on this paradigm. In the realm of visual generation, diffusion models (Ho et al., 2020; Song et al., 2020a; Dhariwal & Nichol, 2021; Song et al., 2020b) have demonstrated superior generative capabilities, producing creative outputs that are virtually indistinguishable from human-generated content, as evidenced by innovations like Sora (Brooks et al., 2024) and Stable Diffusion (Rombach et al., 2022; Podell et al., 2023; Esser et al.). Despite their remarkable success, diffusion models operate in a non-autoregressive manner. They take as input corrupted target sequences of the full length and reconstruct the intended output through *in-place* iterative refinement. The term "in-place" highlights a fundamental distinction from autoregressive models, which provide subsequent prediction, thereby extending the sequence and progressing towards the future. Such variation makes the diffusion model less effective at capturing long-range temporal dependencies in visual data and poses difficulties for developing integrated frameworks capable of seamlessly bridging the vision foundation model with unified multimodality modeling (Dong et al., 2024; Team, 2024; Zhou et al., 2024a; Wang et al., 2024b; Xie et al.,

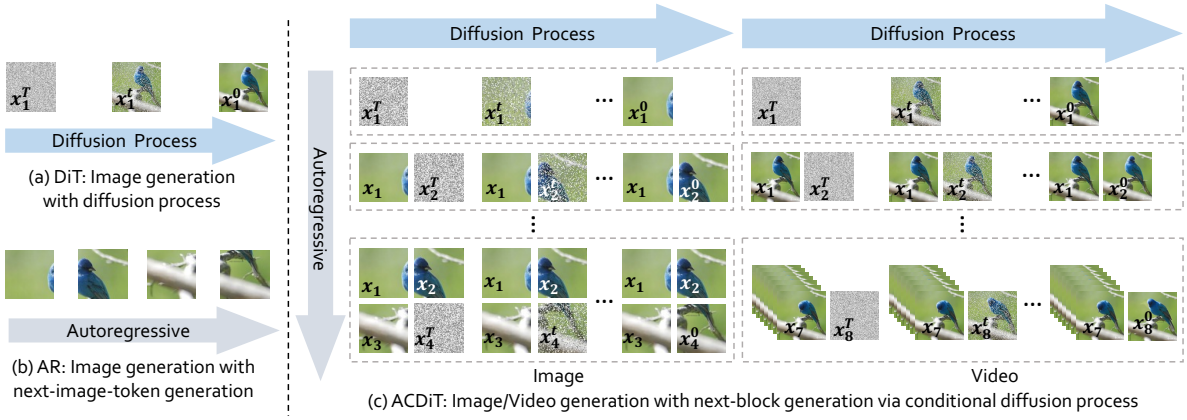

Figure 1: The generation process of ACDiT. Pixels in each block are denoised simultaneously conditioned on **clean context** which are autoregressively generated. The block can be flexibly defined, such as part of pixels in images or several frames in videos.

2024; Wu et al., 2024b) and world model (Yang et al., 2023; Du et al., 2023; Bruce et al., 2024; Zhou et al., 2024b; Ko et al., 2023; Wu et al., 2024a).

To build the visual autoregressive model, existing works convert visual generation tasks into discrete token prediction tasks with vector quantization techniques (Esser et al., 2021; Team, 2024; Wang et al., 2024b; Tian et al., 2024) and training with a next-token prediction objective. However, approaching the continuous distribution requires huge vocabulary sizes and a high utilization rate (Yu et al., 2023b; Weber et al., 2024), which is a complex objective.

In this paper, we propose ACDiT, an **A**utoregressive blockwise **C**onditional **Di**ffusion **T**ransformer that fuses the diffusion process with the autoregressive paradigm. Instead of relying on discrete tokens, we demonstrate that visual autoregressive generation can also be achieved using continuous visual features. At a high level, we extend the autoregressive units from the individual discrete token to blocks, where each block consists of visual patches of flexible size. The generation of each block can be formulated as a conditional diffusion process based on the previous block. As Fig. 1 shows, for image generation, a block represents a small region of the image, whereas in video generation, a block can correspond to a single frame or multiple frames.

ACDiT is easy to implement, as simple as adding a tailored Skip-Causal Attention Mask to the current diffusion transformer (Peebles & Xie, 2022) during training. The inference process is formatted as an iteration between the conditional diffusion denoising process within a block, conditioned on the complete clean context, and autoregressive generation of a new block appended as the new context. In this way, KV-Cache can be used for faster inference. In general, ACDiT offers the following inherent advantages: (i) ACDiT simultaneously learns the causal interdependence across visual blocks with autoregressive modeling and the non-causal dependence within blocks with diffusion modeling. (ii) ACDiT is endowed with clean and continuous visual input, which eliminates the requirement for vector quantization and improves the transfer to visual understanding tasks after being trained with generative objectives. (iii) ACDiT makes full use of KV-Cache for flexible autoregressive generation of any length and can potentially benefit from other latest techniques in text for long video generation.

The effectiveness of ACDiT is primarily validated on visual generation tasks, including both image and video generation tasks, respectively. To further demonstrate its versatility, we also perform experiments on text generation. Experimental results demonstrate that ACDiT outperforms all autoregressive baselines of the same model scale, and achieves visual quality comparable to full-sequence diffusion models while exhibiting higher inference speed when extended to long sequences. It also achieves strong performance on text generation following the discrete diffusion formulation without any specific customization. We hope ACDiT presents a fresh perspective on the visual autoregressive model and paves the way for exploring unified multimodal and world models.

2 Related Work

Diffusion Models. The field of image generation has witnessed remarkable advancements with the introduction of diffusion models (Ho et al., 2020; Song et al., 2020a; Dhariwal & Nichol, 2021; Nichol & Dhariwal, 2021). U-Net (Ronneberger et al., 2015) is the early mainstream choice of network architecture (Song et al., 2020b; Nichol & Dhariwal, 2021; Rombach et al., 2022; Podell et al., 2023). Following that, Transformer (Vaswani et al., 2017) is applied to diffusion models for image generation, with groundbreaking work such as DiT (Peebles & Xie, 2022) and U-ViT (Bao et al., 2023). A series work, including PixArt-$\{\alpha, \delta, \Sigma\}$ (Chen et al., 2023; 2024c;b), demonstrate the capability of DiT on text-to-image tasks. Several studies also apply DiT to video generation, such as Lumiere (Bar-Tal et al., 2024) and Movie Gen (Polyak et al., 2024).

Autoregressive Generation on Discrete Tokens. The iGPT (Chen et al., 2020) first proposes autoregressively generating raw image pixels as a raster-scan sequence. Most visual autoregressive models (Ramesh et al., 2021; Wang et al., 2024b; Yu et al., 2022; Ding et al., 2021; 2022) follow VQGAN (Esser et al., 2021), which pioneers this direction by training an autoregressive transformer on discrete tokens produced by VQVAE (Van Den Oord et al., 2017). LlamaGen (Sun et al., 2024) enhances the image tokenizer and scales up the autoregressive transformers building on the latest Llama architecture (Touvron et al., 2023a). Inspired by RQ-Transformer (Lee et al., 2022), VAR (Tian et al., 2024) proposes the next-scale prediction and obtains good improvement. Some subsequent works (Tian et al., 2024; Li et al., 2024c; Yao et al., 2024) extend next-scale prediction to text-to-image generation.

Autoregressive Generation on Continuous Features. Some recent works make some early exploration on achieving visual autoregressive generation without discrete tokens and combining the advantages of diffusion and autoregressive. Diffusion Forcing (Chen et al., 2024a) trains a causal autoregressive model to generate blocks without fully diffusing past ones and implements it on small RNN. MAR (Li et al., 2024a) proposes the diffusion loss to learn the autoregressive conditional distribution on the head of the main Transformer with a small MLP network. Transfusion (Zhou et al., 2024a) and Monoformer (Zhao et al., 2024a) conduct joint training with language modeling loss and diffusion loss in a single transformer, while within image generation, their design is identical to the standard diffusion model. Dart (Gu et al., 2024) proposes to autoregressively denoise the complete image within in a Transformer. Different from these works, ACDiT redefines the autoregressive unit and generates each block based on the clear past. Block Diffusion (Arriola et al., 2025) also explores an interpolation between autoregressive and diffusion modeling. Their approach focuses solely on text generation. In contrast, ACDiT is designed for visual generation, yet still achieves better results on text generation using our simple and generally effective architecture, without any task-specific modifications to text training.

3 Prerequiste

3.1 Autoregressive Modeling

Autoregression asserts that the value at each timestep is contingent upon its preceding values. This principle is exemplified in autoregressive language models, which iteratively predict the probability distribution of subsequent tokens. Given a sequence of tokens $(x_1, x_2, \ldots, x_n)$, a salient characteristic of autoregression is that the prediction of x_i is only dependent on its prefix $(x_1, x_2, \ldots, x_{i-1})$. Upon determining x_i, it is concatenated with the preceding sequence, thereby forming the conditioning context $(x_1, x_2, \ldots, x_i)$ to predict x_{i+1}. Therefore, the likelihood of sequence can be factorized as:

$$p(x_1, x_2, \ldots, x_N) = \prod_{i=1}^{N} p(x_{i+1}|x_1, x_2, \ldots, x_i). \tag{1}$$

Thanks to the flexibility of self-attention in Transformers, autoregressive models can be effectively implemented by adding a causal attention mask in the Transformer attention block (Vaswani et al., 2017).

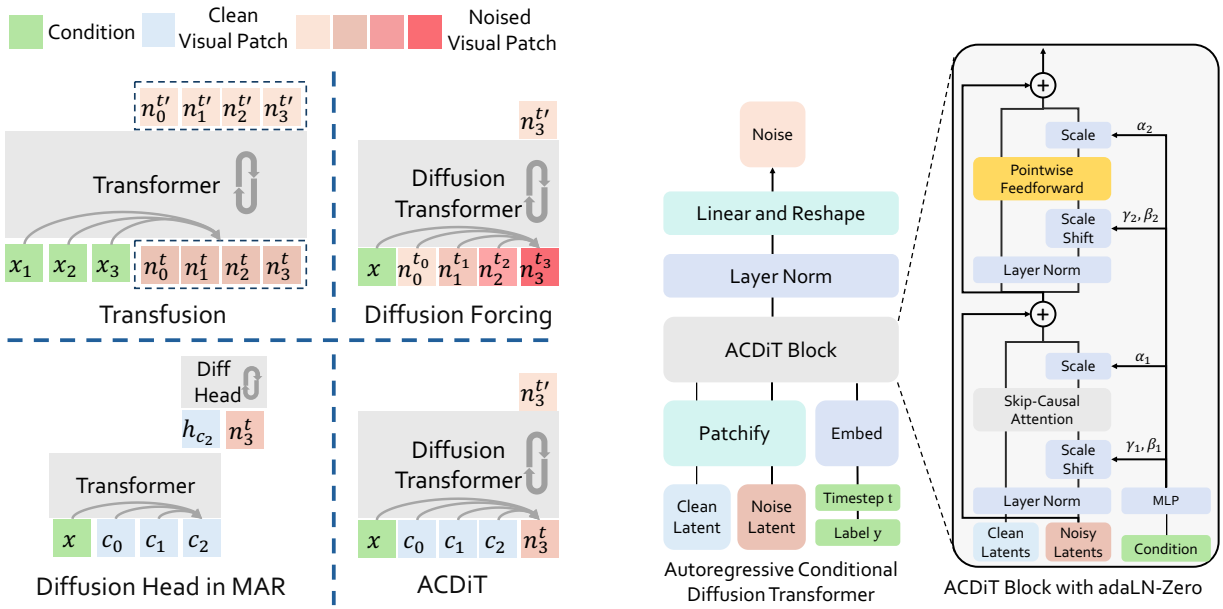

(a) Comparison of model design.

(b) The model architecture of ACDiT.

Figure 2: **(a)**: Comparison between ACDiT with Transfusion (Zhou et al., 2024a), Diffusion Forcing (Chen et al., 2024a) and MAR (Li et al., 2024a).Transfusion does not perform autoregressive modeling within the visual modality. Diffusion Forcing introduces different noise levels across the autoregressive inputs. MAR applies diffusion only on top of the backbone model. ACDiT utilizes the full parameters for both the autoregressive and diffusion process with clean input as context. **(b)**: The model architecture of ACDiT. Both the clean and noisy latent are input, while only the noisy latent interacts with the conditioning information. The SCAM attention mask pattern, shown in Figure 3a, will be applied in the attention block.

3.2 Diffusion

Diffusion models, in contrast, conceptualize a noise-infusion and denoising process, which is defined by gradually adding noise to the initial data $x_0 \sim p(x)$ and training the model to learn the inverse mapping. Formally, the noised data $x^{(t)}$ at each step t is sampled by $q(x^{(t)}|x^{(t-1)}) = \mathcal{N}(x^{(t)}; \sqrt{\alpha^{(t)}}x^{(0)}, (1-\alpha^{(t)})\mathbf{I})$[1], which is equivalent to add a Guassain noise to the previous samples $x^{(t)} = \sqrt{\alpha^{(t)}}x^{(t-1)} + \sqrt{1-\alpha^{(t)}}\epsilon^{(t)}, \epsilon^{(t)} \sim \mathcal{N}(0, \mathbf{I})$. p_θ is trained to learn the reverse process $p_\theta(x^{(t-1)}|x^{(t)}) = \mathcal{N}(\mu_\theta(x^{(t)}), \beta^{(t)}\mathbf{I})$. With the reparameterization trick, the network $\mu_\theta(x^{(t)})$ can be reparameterized as noise prediction network $\epsilon_\theta(x^{(t)})$ and the training objective can be simple as:

$$\mathcal{L}_\theta = \mathbb{E}_{t\sim U[0,1],\epsilon\sim\mathcal{N}(0,I)}||\epsilon_\theta(x^{(t)}, t) - \epsilon^{(t)}||_2. \tag{2}$$

During the inference phase, the denoising process is initialized with a random Gaussian noise sample $x^{(T)}$, followed by T' denoising steps, ultimately yielding a single deterministic sample $\tilde{n}^{(0)}$ from its underlying distribution. Typically, the denoising process in diffusion models operates "in-place", meaning that each new denoising step directly replaces the previous step's input. This differs from autoregressive modeling, where the value of a subsequent step is appended to the existing sequence.

[1]For clarification, we use subscript $_t$ to denote timesteps in autoregressive models and superscript $^{(t)}$ to denote the timesteps in diffusion models.

4 ACDiT

4.1 Desiderata for Autoregressive Diffusion Model

Rather than modeling the full data distribution $p(x)$ directly, autoregressive diffusion aims to learn the conditional distributions for the continuous visual feature $p(x_i|x_{<i})$ through a diffusion process, which is typically represented as categorical distributions over discrete token vocabulary in language models. Combining the Eq.equation 1 and Eq.equation 2, the learning objective of autoregressive diffusion is:

$$\mathcal{L}_\theta = \mathbb{E}_{t\sim U[0,1],\epsilon\sim\mathcal{N}(0,I)} \sum_{i=1}^{N} ||\epsilon_\theta(x_i^{(t)}; t, x_{<i}) - \epsilon^{(t)}||_2, \tag{3}$$

where $\{x_1, x_2, ..., x_N\}$ are N autoregressive units. In the context of visual generation, each unit can flexibly correspond to the continuous visual information of a patch of pixels in an image or a set of frames in a video, depending on the granularity of the representation.

The key difference between Eq. equation 3 and Eq. 2 is that for each input noisy block, the noise prediction network $\epsilon(x_i^{(t)})$ predicts the noise conditioned on their previous clean block. To effectively learn this objective, we need a framework that integrates the strengths of both autoregressive and diffusion models. We identify three critical desiderata the framework should meet:

1. *The generation of future elements should be predicated on a precise representation of antecedent sequences.* This is imperative because any ambiguity in the past inevitably complicates future predictions. This approach preserves the efficacy of autoregressive modeling and potentially facilitates the development of the world model. Furthermore, adherence to this principle enhances performance in discriminative tasks (e.g., visual understanding), as these tasks necessitate the input of all observable features into the model.

2. *Both the autoregressive modeling and the denoising process should optimally utilize the entire parameter space of the neural network.* In an elegant fusion of autoregressive models and diffusion, neither component should be relegated to an auxiliary role. Instead, they should function as integral and complementary elements of the system.

3. *The denoising process should directly attend comprehensively to the entire sequence of past sequences.* Otherwise, the conditioning input to the denoising process would be required to fully encapsulate all prior information, imposing an unrealistic burden on the bottleneck context vector to losslessly compress the context feature into one vector. A holistic input of all past information in each denoise step ensures a more effective processing of temporal dependencies.

Based on these desiderata, we analyze representative autoregressive diffusion methods. **Diffusion-Forcing** (Chen et al., 2024a) proposes to use different-level random noise in different positions of a sequence. Thus, in the inference process, denoising subsequent positions from a clean past can be seen as a special case of denoising different levels of noise. Their method does not meet the first desideratum. In the training process, the future is not predicted from the precise representation of the past. In **MAR** (Li et al., 2024a), the diffusion process is trained based on the block in the last position, which does not satisfy the third desideratum. Moreover, the diffusion process sorely leverages the head part of the network, which conflicts with the second desideratum. To address suboptimal performance due to the causal direction based on this design, MAR incorporates bidirectional attention, which requires recomputing attention at each step and prevents the use of KV-cache during inference. In **Transfusion** (Zhou et al., 2024a) and **Monoformer** (Zhao et al., 2024a), the autoregressive generation is restricted to the textual modality and is not applied within the visual modality. Image generation in these models follows the standard diffusion process conditioned on preceding text inputs, without incorporating autoregressive prediction over visual patches. Moreover, in visual understanding tasks or multi-image generation settings, subsequent text and images attend to the noisy version of the preceding image, which conflicts with the first desideratum. To mitigate this issue, these models reduce the noise schedule, i.e., halving the maximum number of diffusion steps from 1000 to 500, in 20% of image-captioning pairs, which is not an optimal strategy. See the visual comparison of these models in Fig. 2a.

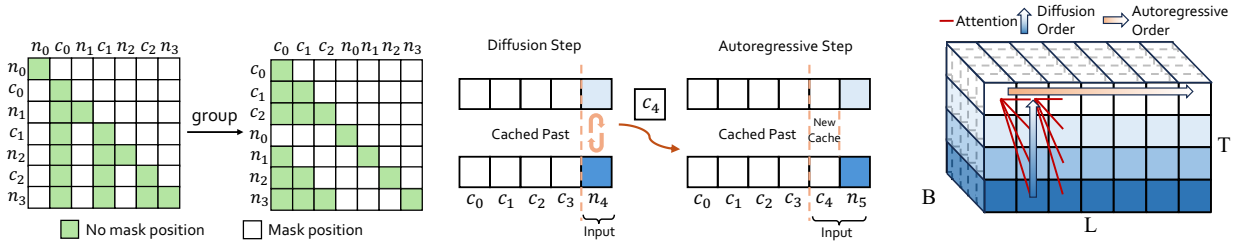

(a) Skip-Causal Attention Mask. (b) Inference process of ACDiT. (c) 3D view of ACDiT.

Figure 3: **(a)**: For each noised block n_i, it can only attend previous clean block $\{c_0, c_1, \ldots, c_{i-1}\}$ and itself. Each clean block c_i only attends to the previous clean blocks. **(b)**: ACDiT can effectively utilize the KV-Cache during inference. **(c)**: the 3D view of ACDiT, where B, L, T denote the block size, number of blocks, and denoising time steps, respectively. The darker color denotes higher noise.

4.2 Framework

To satisfy the desiderata discussed above, we propose a versatile framework for autoregressive diffusion called ACDiT. For generality, ACDiT runs block-wise autoregression instead of token-wise autoregression. We identify two kinds of blocks c_i and n_i. For each autoregressive unit x_i, c_i corresponds to the clean version x_i, n_i corresponds to the corrupted version $x_i^{(t)}$. ACDiT learns the conditional noise prediction network $\epsilon_\theta(n_i^{(t)}; t, c_{<i})$ with Eq. equation 3.

To effectively learn this objective within one transformer network, we can conceptualize all n_i and all c_i as separate positions, effectively transforming the dependency structure into an attention pattern between different positions. We designate this attention pattern as the Skip-Causal Attention Mask (SCAM), shown in Figure 3a. The figure elucidates that n_i attends to all preceding clean blocks $\{c_j | j = 0, ..., i-1\}$ and itself, while c_i also attends to all preceding clean blocks $\{c_j | j = 0, ..., i-1\}$ and itself. In training, for simplicity, we can group attention mechanisms as illustrated in the right matrix of Figure 3a. Suppose the number of blocks is N, then the unmasked positions form two triangular matrices with length $N-1$, complemented by a diagonal matrix with length N.

During the inference phase, each autoregressive step executes a conditional diffusion process for n_i based on $\{c_0, c_1, ..., c_{i-1}\}$'s KV-Cache. Upon finishing denoising, it is appended to the clean sequence as c_i followed by the maximal noisy version of the next block n_{i+1}. The key-value tensor will be computed for these two blocks, and the key-value tensor of the clean block c_i will be kept in KV-Cache. All noisy version of n_i is disregarded. The process is visualized in Figure 3b. A three-dimensional view is presented in Figure 3c. By interpolating between full-sequence diffusion and autoregressive paradigms, ACDiT enjoys flexibility and expressivity, enabling it to generate video of any length utilizing the latest long-context techniques developed for language models.

4.3 Positional Encoding

ACDiT is designed to be versatile, capable of handling one-, two-, three-, or even higher-dimensional data, including but not limited to text (1D), images (2D), and video (3D). For any given dimension of data, the position of that data is a critical attribute that must be made known to the model. This positional awareness enables the model to contextualize its current focus relative to historical data. In the domain of textual data, the Rotary Position Embedding (RoPE) (Su et al., 2024) has gained widespread adoption as an effective relative positional encoding method. To address the challenges posed by multi-dimensional positional indices, we introduce RoPE-ND, a natural extension of RoPE.

For a token of a D dimensional data, its positional index is $[m_1, m_2, ..., m_D]$. Given query and key vectors in the Transformer's attention module, we partition the hidden dimension into D segments. It is imperative that each segment's hidden dimension be an even number. For each segment j, we apply a RoPE with a

specific base b_j, as defined in the following equation:

$$\mathbf{R} = \begin{bmatrix} \mathbf{R}^{d_1}_{\Theta_1,m_1} & 0 & \cdots & 0 \\ 0 & \mathbf{R}^{d_2}_{\Theta_2,m_2} & \cdots & 0 \\ \vdots & \vdots & \ddots & \vdots \\ 0 & 0 & \cdots & \mathbf{R}^{d_D}_{\Theta_D,m_D} \end{bmatrix}, \tag{4}$$

where each $\mathbf{R}^{d_j}_{\Theta_j,m_j}$ represents a d_j-dimensional rotary matrix[2] with rotation angles $\Theta_j = \{b_j^{-2(i-1)/d_j}, i \in [1, 2, \cdots, \frac{d_j}{2}]\}$. The base b_j is empirically determined as $100\lceil\frac{8L_j}{100\pi}\rceil$, where L_j denotes the maximum position index in dimension j. This formulation ensures that the highest wavelength of RoPE is approximately eight times the maximum position, thereby mitigating rapid decay in long-term dependencies. It is worth noting that ACDiT inherently supports length extrapolation (Su et al., 2024), although a comprehensive exploration of this falls beyond the present work.

4.4 Efficiency Analysis and Block Size Choice

We provide a brief analysis of the computational efficiency of ACDiT in terms of floating-point operations (FLOPS). The full derivation and more analysis are discussed in the Appendix A. We first assume that denoising each block requires the same number of time steps T as the full sequence diffusion, despite that when the block size is small, it may require fewer denoising steps, thus making ACDiT potentially more efficient. Let L denote the sequence length, h the hidden dimension, θ the number of parameters in a transformer layer, and B the block size used in ACDiT. The FLOPS for standard full-sequence diffusion is $F_{\text{full}} = 2L\theta + 4hL^2$. With KV-Cache, ACDiT reduces the attention cost to $2hL^2 + 2hLB$. The relative FLOPS savings is: $\frac{F_{\text{saved}}}{F_{\text{full}}} = \frac{1-\frac{B}{L}}{2+\frac{\theta}{hL}}$. This indicates that ACDiT can reduce per-layer FLOPS by up to 50% when $L \gg B$.

4.5 Model Architecture and Implementation

As shown in Fig. 2b, ACDiT mainly inherits the main architecture of DiT. We replace the original bidirectional attention with the proposed SCAM attention pattern to process the clean and noisy latent. In addition, we replace the absolute position embedding and Layer Normalization with RoPE (Su et al., 2024) and RMSNorm (Touvron et al., 2023a), respectively. We use QK-norms for stable training. The additional condition, including timesteps and labels, is injected into the model with AdaLN-Zero only on the noise part.

We explore 4 different model sizes, as shown in Table 5. In the image generation task, we set the patch size as 1 and the autoregressive unit block size as $256 = 16 \times 16$. ACDiT is trained on ImageNet for 1.2M iterations with a batch size of 1024. We use the AdamW optimizer (Loshchilov, 2017) and WSD (Warmup Steady Decay) learning rate scheduling (Hu et al., 2024). We sample images with DPM-Solver (Lu et al., 2022) for 25 steps within each block and use classifier-free guidance (Ho & Salimans, 2022) with a guidance scale of 1.5. In video generation, we sample 16 frames from each video and set the patch size as 2 and the block size as $1024 = 256 \times 4$. We train ACDiT on UCF-101 for 400K iterations with a batch size of 96. The classifier-free guidance scale is 2.5. See more details at Appendix 4.5.

5 Experiments

We mainly experiment on the ImageNet (Russakovsky et al., 2015) dataset with 256×256 resolution and the UCF-101 (Soomro et al., 2012) dataset with 16 frames for image generation and video generation, respectively. In addition, we also validate the generality of ACDiT on text generation.

[2]See a detailed explanation in the Equation 15 in (Su et al., 2024).

Table 1: Image generation results on ImageNet 256x256.

Model	Type	Latent	KV-Cache	Params	FID↓	IS↑	Pre↑	Rec↑
ADM (Dhariwal & Nichol, 2021)	Diff.	-	-	554M	10.94	101.0	0.69	0.63
LDM-4-G (Rombach et al., 2022)	Diff.	Cont.	-	400M	3.60	247.7	-	-
DiT-L/2 (Peebles & Xie, 2022)	Diff.	Cont.	-	458M	5.02	167.2	0.75	0.57
DiT-XL/2 (Peebles & Xie, 2022)	Diff.	Cont.	-	675M	2.27	278.2	0.83	0.57
MaskGIT (Weber et al., 2024)	Mask.	Disc.	-	227M	6.18	316.2	0.83	0.58
MAGE (Li et al., 2023)	Mask.	Disc.	-	230M	6.93	195.8	-	-
VQGAN (Esser et al., 2021)	AR	Disc.	✓	1.4B	15.78	78.3	-	-
RQTran (Lee et al., 2022)	AR	Disc.	✓	3.8B	7.55	134.0	-	-
VAR-d16 (Tian et al., 2024)	VAR	Disc.	✓	310M	3.30	274.4	0.84	0.51
VAR-d20 (Tian et al., 2024)	VAR	Disc.	✓	600M	2.57	302.6	0.83	0.56
LlamaGen-L (Sun et al., 2024)	AR	Disc.	✓	343M	3.07	256.1	0.83	0.52
LlamaGen-XL (Sun et al., 2024)	AR	Disc.	✓	775M	2.62	244.1	0.80	0.57
LlamaGen-XXL (Sun et al., 2024)	AR	Disc.	✓	1.4B	2.34	253.9	0.80	0.59
ImageFolder (Li et al., 2024b)	AR	Disc.	✓	362M	2.60	295.0	0.75	0.63
LlamaGen+NPP (Pang et al., 2024)	AR	Cont.	✓	1.4B	2.55	282.0	0.84	0.56
MAR-L (Tian et al., 2024)	AR	Cont.	✓	479M	4.07	232.4	-	-
MAR-L (Tian et al., 2024)	MAR	Cont.	-	479M	1.78	296.0	0.81	0.60
MonoFormer (Zhao et al., 2024a)	AR+Diff	Cont.	-	1.1B	2.57	272.6	0.84	0.56
Dart (Gu et al., 2025)	AR+Diff	Cont.	✓	820M	3.82	263.8	-	-
ACDiT-L	AR+Diff	Cont.	✓	460M	2.53	262.9	0.82	0.55
ACDiT-XL	AR+Diff	Cont.	✓	677M	2.45	267.4	0.82	0.57
ACDiT-H	AR+Diff	Cont.	✓	954M	2.37	273.3	0.82	0.57

5.1 Main Results

Image Generation. We report the FID-50K (Heusel et al., 2017), Inception Score (Salimans et al., 2016), Precision and Recall (Kynkäänniemi et al., 2019) of ACDiT and baselines in Table 1. Compared with previous autoregressive models and masked generative models utilizing discrete tokens, such as VQGAN, VAR, LlamaGen, and MaskGIT, ACDiT consistently achieves superior performance with lower FID scores at comparable model scales. Notably, ACDiT-XL achieves 2.45 FID scores, outperforming both LlamaGen-XXL and VAR-d20 with similar parameters. Additionally, when compared to the MAR-L **variant that does not recompute attention**, ACDiT-L significantly improves performance across all metrics, specifically improving FID from 4.07 to 2.53. Compared with other autoregressive diffusion methods, such as Monoformer (Zhao et al., 2024a) and Dart (Gu et al., 2024), ACDiT has a significantly superior performance. When compared with leading diffusion-based methods, ACDiT also demonstrates competitive performance. For instance, despite not employing full-sequence attention, ACDiT models achieve results close to DiT-XL. In general, these results highlight the distinct advantages of ACDiT over other baselines with the continuous latent representation and KV-Cache. Qualitative results are presented in the Appendix C.

Video Generation. Different from image generation, video inherently includes a temporal dimension, making it more well-suited to autoregressive modeling. The FVD metric on UCF-101 for class-conditional video generation is reported in Table 2. With hybrid AR+Diff architecture, ACDiT-H achieves much lower FVD than other diffusion-based and autoregressive methods, even outperforming MAGVIT-AR and MAGVITv2-AR, which utilize a closed-source, specially designed video tokenizer. In contrast, ACDiT simplifies the process by directly using an open-sourced image VAE. Although MAGVIT with masked generative methods has a lower FVD than ACDiT, they rely on in-place operation to generate a video similar to the diffusion model. This constraint limits their ability to generalize to long video generation and build world models. Compared to image generation, ACDiT demonstrates a greater potential in the more complex domain of video generation, where longer visual sequences and temporal information are critical. Qualitative results are presented in the Appendix C.

Table 2: Video generation results on the UCF-101 dataset. ACDiT-XL-LT means ACDiT-XL trained for longer epochs.

Model	Type	Params	FVD↓
LVDM (He et al., 2022b)	Diff.	437M	372
Latte (Ma et al., 2024)	Diff.	674M	478
Video-LaVIT (Jin et al., 2024)	Diff.	7B	281
MagDiff (Zhao et al., 2024b)	Diff.	2B	340
Matten (Gao et al., 2024)	Diff.	853M	211
VideoFusion (Luo et al., 2023)	Diff.	510M	173
MMVG (Fu et al., 2023)	Mask.	230M	328
MAGVIT (Yu et al., 2023a)	Mask.	306M	76
MAGVITv2 (Yu et al., 2023b)	Mask.	307M	58
TATS (Ge et al., 2022)	AR	331M	332
CogVideo (Hong et al., 2022)	AR	9.4B	626
MAGVIT-AR (Yu et al., 2023a)	AR	306M	265
MAGVITv2-AR (Yu et al., 2023b)	AR	307M	109
OmniTokenizer (Wang et al., 2024a)	AR	650M	191
ACDiT-XL	AR+Diff.	677M	111
ACDiT-H	AR+Diff.	954M	104
ACDiT-H-LT	AR+Diff.	954M	90

Table 3: Classification accuracy on ImageNet.

Model	Type	Top-1 Acc
ViT-H (Dosovitskiy, 2020)	Supervised	83.1
MAGE (Li et al., 2023)	Masked	84.3
MAE (He et al., 2022a)	Masked	85.9
iGPT (Chen et al., 2020)	Generative	72.6
DiT-XL (Peebles & Xie, 2022)	Generative	82.8
ACDiT-XL	Generative	84.0

Table 4: Test perplexities on OpenWebText.

		PPL (↓)
Autoregressive		
AR (Sahoo et al., 2024)		17.54
Diffusion		
SEDD (Lou et al., 2023)		$\leq$ 24.10
MDLM (Sahoo et al., 2024)		$\leq$ 22.98
Block-wise diffusion		
BD3-LMs (Arriola et al., 2025)	$L' = 16$	$\leq$ 22.27
	$L' = 8$	$\leq$ 21.68
ACDiT	$L' = 256$	$\leq$ 22.98
	$L' = 128$	$\leq$ 22.82
	$L' = 8$	$\leq$ 21.59

Text Generation. ACDiT is a general, modality-agnostic framework. To illustrate its versatility, we implement ACDiT for language modeling with discrete diffusion methods following previous literature (Sahoo et al., 2024; Shi et al., 2024). Despite conceptual similarity to blockwise discrete approaches (Arriola et al., 2025), our effective positional embedding implementation (e.g., RoPE-ND; Sec. 4.3) enables ACDiT to achieve comparable performance across various block sizes as shown in Tab. 4 without any customized variance reduction or noise schedules as proposed in (Arriola et al., 2025). These advantages highlight the potential of ACDiT as a general and powerful generative modeling framework.

Image Representation. We assess the capability of ACDiT in image representation, which is essential for building a unified visual understanding and generation model. We finetune ACDiT-XL and DiT-XL on ImageNet using classification loss for 100 epochs and report the Top-1 accuracy in Table 3. ACDiT outperforms DiT-XL, highlighting the advantage of using clean latents, which help the model to learn better representations compared to using only noisy latent inputs. Additionally, ACDiT matches the Top-1 accuracy of MAGE (Li et al., 2023), while offering superior generation performance.

5.2 Analysis

Trade off of block size. Fig. 4 illustrates the trend of trade-off under different sequence lengths and block sizes in image and video generation tasks on ACDiT-B. The FID curve indicates that for image generation, directly increasing the autoregressive length leads to a decline in image quality, since each patch receives less attention information on average. However, we can mitigate this decline by increasing the total sequence length, which means reducing the patch size. For video generation, ACDiT shows more advantages due to the inherent temporal dependence of videos. The FVD curve demonstrates that increasing autoregressive length has minimal effect on the video quality, even with slight improvement. As for efficiency, we test the sampling time for various sequence lengths with a batch size of 4 on an NVIDIA A100 GPU. Fig. 5 shows that as the sequence length increases, particularly beyond 16k, full-sequence attention (AR length of 1) becomes very time-consuming, necessitating the autoregressive generation.

Scaling Performance. We present the scaling performance of ACDiT in Fig. 6a. For a fair comparison with DiT, we use the same batch size and learning rate as DiT in these training sessions. When increasing the model size, ACDiT shows consistent improvement in image quality across all autoregressive lengths, sharing

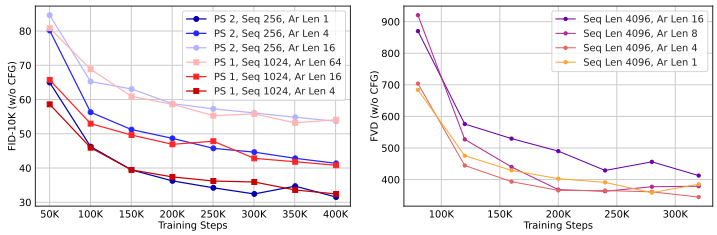

Figure 4: FID and FVD curves of ACDiT-B over training steps with different sequence lengths and autoregressive lengths. PS means patch size.

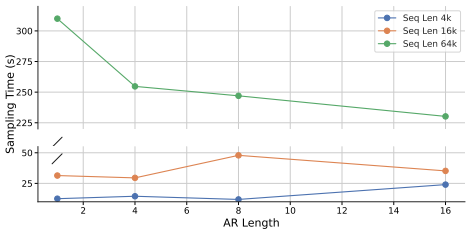

Figure 5: The change of inference time in different autoregressive lengths under varied total sequence length.

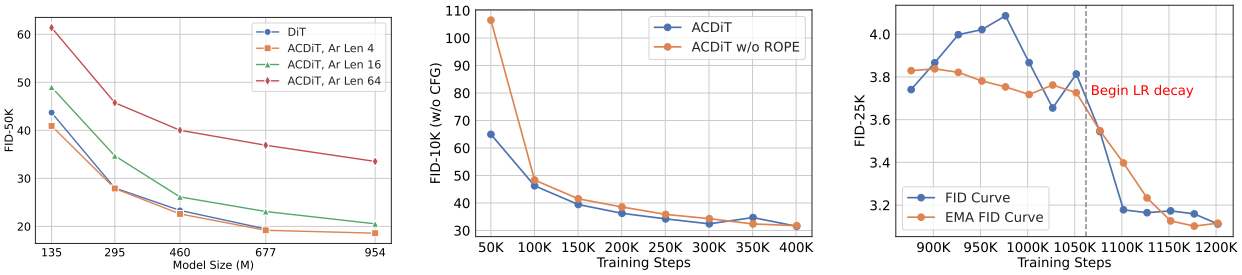

(a) Scaling performance of ACDiT. (b) Ablation study for ROPE-ND. (c) FID curve of last 30% training.

Figure 6: **(a)**: ACDiT shows scaling performance similar to DiT. **(b)**: ROPE-ND has a consistent improvement in the generation quality. **(c)**: FID score sharply drops with the learning rate beginning to decay when using the WSD scheduler.

a similar scaling trend with DiT. Notably, the improvement is more pronounced with longer autoregressive lengths. We hypothesize that this is due to reduced accumulation of errors when scaling the model size.

ROPE-ND. We ablate the effectiveness of ROPE-ND positional embedding on image generation. As shown in Fig 6b, adding ROPE-ND results in consistent improvements in FID score.

Training dynamics of WSD scheduler. We utilize the WSD learning rate scheduler (Hu et al., 2024). WSD scheduler uses a constant learning rate during main training, while allowing divergence at any point with a rapidly decaying learning rate based on compute budget. As Fig. 6c shows, the FID remains almost converged during the constant learning rate state, while sharply dropping after the learning decays, similar to the loss curve when using the WSD scheduler in LLM training. To the best of our knowledge, we are the first to validate the effectiveness of the WSD scheduler in visual generation.

6 Conclusion

In this paper, we propose ACDiT that interpolates the autoregressive modeling and diffusion transformers. With a simple but novel design of attention mask, ACDiT can achieve autoregressive generation on any length while maintaining a clear latent input potentially for adding a visual understanding task. By combining the advantages of both autoregressive and diffusion models, we demonstrate the performance and efficiency of ACDiT in both image and video generation tasks. We hope ACDiT can shed light on designing the new visual autoregressive model and building a unified multimodal model in the future.

References

Josh Achiam, Steven Adler, Sandhini Agarwal, Lama Ahmad, Ilge Akkaya, Florencia Leoni Aleman, Diogo Almeida, Janko Altenschmidt, Sam Altman, Shyamal Anadkat, et al. Gpt-4 technical report. *arXiv preprint arXiv:2303.08774*, 2023.

Marianne Arriola, Aaron Gokaslan, Justin T Chiu, Zhihan Yang, Zhixuan Qi, Jiaqi Han, Subham Sekhar Sahoo, and Volodymyr Kuleshov. Block diffusion: Interpolating between autoregressive and diffusion language models. *arXiv preprint arXiv:2503.09573*, 2025.

Jinze Bai, Shuai Bai, Yunfei Chu, Zeyu Cui, Kai Dang, Xiaodong Deng, Yang Fan, Wenbin Ge, Yu Han, Fei Huang, et al. Qwen technical report. *arXiv preprint arXiv:2309.16609*, 2023.

Fan Bao, Shen Nie, Kaiwen Xue, Yue Cao, Chongxuan Li, Hang Su, and Jun Zhu. All are worth words: A vit backbone for diffusion models. In *CVPR*, 2023.

Omer Bar-Tal, Hila Chefer, Omer Tov, Charles Herrmann, Roni Paiss, Shiran Zada, Ariel Ephrat, Junhwa Hur, Yuanzhen Li, Tomer Michaeli, et al. Lumiere: A space-time diffusion model for video generation. *arXiv preprint arXiv:2401.12945*, 2024.

Tim Brooks, Bill Peebles, Connor Holmes, Will DePue, Yufei Guo, Li Jing, David Schnurr, Joe Taylor, Troy Luhman, Eric Luhman, Clarence Ng, Ricky Wang, and Aditya Ramesh. Video generation models as world simulators. 2024. URL https://openai.com/research/video-generation-models-as-world-simulators.

Tom B Brown. Language models are few-shot learners. *arXiv preprint arXiv:2005.14165*, 2020.

Jake Bruce, Michael D Dennis, Ashley Edwards, Jack Parker-Holder, Yuge Shi, Edward Hughes, Matthew Lai, Aditi Mavalankar, Richie Steigerwald, Chris Apps, et al. Genie: Generative interactive environments. In *Forty-first International Conference on Machine Learning*, 2024.

Boyuan Chen, Diego Marti Monso, Yilun Du, Max Simchowitz, Russ Tedrake, and Vincent Sitzmann. Diffusion forcing: Next-token prediction meets full-sequence diffusion. *arXiv preprint arXiv:2407.01392*, 2024a.

Junsong Chen, Jincheng Yu, Chongjian Ge, Lewei Yao, Enze Xie, Yue Wu, Zhongdao Wang, James Kwok, Ping Luo, Huchuan Lu, and Zhenguo Li. Pixart-α: Fast training of diffusion transformer for photorealistic text-to-image synthesis, 2023.

Junsong Chen, Chongjian Ge, Enze Xie, Yue Wu, Lewei Yao, Xiaozhe Ren, Zhongdao Wang, Ping Luo, Huchuan Lu, and Zhenguo Li. Pixart-\sigma: Weak-to-strong training of diffusion transformer for 4k text-to-image generation. *arXiv preprint arXiv:2403.04692*, 2024b.

Junsong Chen, Yue Wu, Simian Luo, Enze Xie, Sayak Paul, Ping Luo, Hang Zhao, and Zhenguo Li. Pixart-{\delta}: Fast and controllable image generation with latent consistency models. *arXiv preprint arXiv:2401.05252*, 2024c.

Lili Chen, Kevin Lu, Aravind Rajeswaran, Kimin Lee, Aditya Grover, Misha Laskin, Pieter Abbeel, Aravind Srinivas, and Igor Mordatch. Decision transformer: Reinforcement learning via sequence modeling. *Advances in neural information processing systems*, 34:15084–15097, 2021.

Mark Chen, Alec Radford, Rewon Child, Jeffrey Wu, Heewoo Jun, David Luan, and Ilya Sutskever. Generative pretraining from pixels. In *International conference on machine learning*, pp. 1691–1703. PMLR, 2020.

Prafulla Dhariwal and Alexander Nichol. Diffusion models beat gans on image synthesis. *Advances in neural information processing systems*, 34:8780–8794, 2021.

Ming Ding, Zhuoyi Yang, Wenyi Hong, Wendi Zheng, Chang Zhou, Da Yin, Junyang Lin, Xu Zou, Zhou Shao, Hongxia Yang, et al. Cogview: Mastering text-to-image generation via transformers. *Advances in neural information processing systems*, 34:19822–19835, 2021.

Ming Ding, Wendi Zheng, Wenyi Hong, and Jie Tang. Cogview2: Faster and better text-to-image generation via hierarchical transformers. *Advances in Neural Information Processing Systems*, 35:16890–16902, 2022.

Runpei Dong, Chunrui Han, Yuang Peng, Zekun Qi, Zheng Ge, Jinrong Yang, Liang Zhao, Jianjian Sun, Hongyu Zhou, Haoran Wei, Xiangwen Kong, Xiangyu Zhang, Kaisheng Ma, and Li Yi. DreamLLM: Synergistic multimodal comprehension and creation. In *The Twelfth International Conference on Learning Representations*, 2024. URL https://openreview.net/forum?id=y01KGvd9Bw.

Alexey Dosovitskiy. An image is worth 16x16 words: Transformers for image recognition at scale. *arXiv preprint arXiv:2010.11929*, 2020.

Yilun Du, Mengjiao Yang, Pete Florence, Fei Xia, Ayzaan Wahid, Brian Ichter, Pierre Sermanet, Tianhe Yu, Pieter Abbeel, Joshua B Tenenbaum, et al. Video language planning. *arXiv preprint arXiv:2310.10625*, 2023.

Patrick Esser, Sumith Kulal, Andreas Blattmann, Rahim Entezari, Jonas Müller, Harry Saini, Yam Levi, Dominik Lorenz, Axel Sauer, Frederic Boesel, et al. Scaling rectified flow transformers for high-resolution image synthesis. In *Forty-first International Conference on Machine Learning*.

Patrick Esser, Robin Rombach, and Bjorn Ommer. Taming transformers for high-resolution image synthesis. In *Proceedings of the IEEE/CVF conference on computer vision and pattern recognition*, pp. 12873–12883, 2021.

Tsu-Jui Fu, Licheng Yu, Ning Zhang, Cheng-Yang Fu, Jong-Chyi Su, William Yang Wang, and Sean Bell. Tell me what happened: Unifying text-guided video completion via multimodal masked video generation. In *Proceedings of the IEEE/CVF Conference on Computer Vision and Pattern Recognition*, pp. 10681–10692, 2023.

Yu Gao, Jiancheng Huang, Xiaopeng Sun, Zequn Jie, Yujie Zhong, and Lin Ma. Matten: Video generation with mamba-attention. *arXiv preprint arXiv:2405.03025*, 2024.

Songwei Ge, Thomas Hayes, Harry Yang, Xi Yin, Guan Pang, David Jacobs, Jia-Bin Huang, and Devi Parikh. Long video generation with time-agnostic vqgan and time-sensitive transformer. In *European Conference on Computer Vision*, pp. 102–118. Springer, 2022.

Jiatao Gu, Yuyang Wang, Yizhe Zhang, Qihang Zhang, Dinghuai Zhang, Navdeep Jaitly, Josh Susskind, and Shuangfei Zhai. Dart: Denoising autoregressive transformer for scalable text-to-image generation. *arXiv preprint arXiv:2410.08159*, 2024.

Jiatao Gu, Yuyang Wang, Yizhe Zhang, Qihang Zhang, Dinghuai Zhang, Navdeep Jaitly, Joshua M. Susskind, and Shuangfei Zhai. Denoising autoregressive transformers for scalable text-to-image generation. In *The Thirteenth International Conference on Learning Representations*, 2025. URL https://openreview.net/forum?id=amDkNPVWcn.

David Ha and Jürgen Schmidhuber. World models. *arXiv preprint arXiv:1803.10122*, 2018.

Kaiming He, Xinlei Chen, Saining Xie, Yanghao Li, Piotr Dollár, and Ross Girshick. Masked autoencoders are scalable vision learners. In *Proceedings of the IEEE/CVF conference on computer vision and pattern recognition*, pp. 16000–16009, 2022a.

Yingqing He, Tianyu Yang, Yong Zhang, Ying Shan, and Qifeng Chen. Latent video diffusion models for high-fidelity long video generation. 2022b.

Martin Heusel, Hubert Ramsauer, Thomas Unterthiner, Bernhard Nessler, and Sepp Hochreiter. Gans trained by a two time-scale update rule converge to a local nash equilibrium. *Advances in neural information processing systems*, 30, 2017.

Jonathan Ho and Tim Salimans. Classifier-free diffusion guidance. *arXiv preprint arXiv:2207.12598*, 2022.

Jonathan Ho, Ajay Jain, and Pieter Abbeel. Denoising diffusion probabilistic models. *Advances in neural information processing systems*, 33:6840–6851, 2020.

Wenyi Hong, Ming Ding, Wendi Zheng, Xinghan Liu, and Jie Tang. Cogvideo: Large-scale pretraining for text-to-video generation via transformers. *arXiv preprint arXiv:2205.15868*, 2022.

Shengding Hu, Yuge Tu, Xu Han, Chaoqun He, Ganqu Cui, Xiang Long, Zhi Zheng, Yewei Fang, Yuxiang Huang, Weilin Zhao, et al. Minicpm: Unveiling the potential of small language models with scalable training strategies. *arXiv preprint arXiv:2404.06395*, 2024.

Albert Q Jiang, Alexandre Sablayrolles, Arthur Mensch, Chris Bamford, Devendra Singh Chaplot, Diego de las Casas, Florian Bressand, Gianna Lengyel, Guillaume Lample, Lucile Saulnier, et al. Mistral 7b. *arXiv preprint arXiv:2310.06825*, 2023.

Yang Jin, Zhicheng Sun, Kun Xu, Liwei Chen, Hao Jiang, Quzhe Huang, Chengru Song, Yuliang Liu, Di Zhang, Yang Song, et al. Video-lavit: Unified video-language pre-training with decoupled visual-motional tokenization. In *International Conference on Machine Learning*, pp. 22185–22209. PMLR, 2024.

Diederik P Kingma. Auto-encoding variational bayes. *arXiv preprint arXiv:1312.6114*, 2013.

Po-Chen Ko, Jiayuan Mao, Yilun Du, Shao-Hua Sun, and Joshua B Tenenbaum. Learning to act from actionless videos through dense correspondences. *arXiv preprint arXiv:2310.08576*, 2023.

Tuomas Kynkäänniemi, Tero Karras, Samuli Laine, Jaakko Lehtinen, and Timo Aila. Improved precision and recall metric for assessing generative models. *Advances in neural information processing systems*, 32, 2019.

Doyup Lee, Chiheon Kim, Saehoon Kim, Minsu Cho, and Wook-Shin Han. Autoregressive image generation using residual quantization. In *Proceedings of the IEEE/CVF Conference on Computer Vision and Pattern Recognition*, pp. 11523–11532, 2022.

Yaniv Leviathan, Matan Kalman, and Yossi Matias. Fast inference from transformers via speculative decoding. In *International Conference on Machine Learning*, pp. 19274–19286. PMLR, 2023.

Tianhong Li, Huiwen Chang, Shlok Mishra, Han Zhang, Dina Katabi, and Dilip Krishnan. Mage: Masked generative encoder to unify representation learning and image synthesis. In *Proceedings of the IEEE/CVF Conference on Computer Vision and Pattern Recognition*, pp. 2142–2152, 2023.

Tianhong Li, Yonglong Tian, He Li, Mingyang Deng, and Kaiming He. Autoregressive image generation without vector quantization. *arXiv preprint arXiv:2406.11838*, 2024a.

Xiang Li, Hao Chen, Kai Qiu, Jason Kuen, Jiuxiang Gu, Bhiksha Raj, and Zhe Lin. Imagefolder: Autoregressive image generation with folded tokens. *arXiv preprint arXiv:2410.01756*, 2024b.

Xiang Li, Kai Qiu, Hao Chen, Jason Kuen, Zhe Lin, Rita Singh, and Bhiksha Raj. Controlvar: Exploring controllable visual autoregressive modeling. *arXiv preprint arXiv:2406.09750*, 2024c.

I Loshchilov. Decoupled weight decay regularization. *arXiv preprint arXiv:1711.05101*, 2017.

Aaron Lou, Chenlin Meng, and Stefano Ermon. Discrete diffusion modeling by estimating the ratios of the data distribution. *arXiv preprint arXiv:2310.16834*, 2023.

Cheng Lu, Yuhao Zhou, Fan Bao, Jianfei Chen, Chongxuan Li, and Jun Zhu. Dpm-solver: A fast ode solver for diffusion probabilistic model sampling in around 10 steps. *Advances in Neural Information Processing Systems*, 35:5775–5787, 2022.

Zhengxiong Luo, Dayou Chen, Yingya Zhang, Yan Huang, Liang Wang, Yujun Shen, Deli Zhao, Jingren Zhou, and Tieniu Tan. Videofusion: Decomposed diffusion models for high-quality video generation. *arXiv preprint arXiv:2303.08320*, 2023.

Xin Ma, Yaohui Wang, Gengyun Jia, Xinyuan Chen, Ziwei Liu, Yuan-Fang Li, Cunjian Chen, and Yu Qiao. Latte: Latent diffusion transformer for video generation. *arXiv preprint arXiv:2401.03048*, 2024.

Volodymyr Mnih. Playing atari with deep reinforcement learning. *arXiv preprint arXiv:1312.5602*, 2013.

Alexander Quinn Nichol and Prafulla Dhariwal. Improved denoising diffusion probabilistic models. In *International conference on machine learning*, pp. 8162–8171. PMLR, 2021.

Yatian Pang, Peng Jin, Shuo Yang, Bin Lin, Bin Zhu, Zhenyu Tang, Liuhan Chen, Francis EH Tay, Ser-Nam Lim, Harry Yang, et al. Next patch prediction for autoregressive visual generation. *arXiv preprint arXiv:2412.15321*, 2024.

Adam Paszke, Sam Gross, Francisco Massa, Adam Lerer, James Bradbury, Gregory Chanan, Trevor Killeen, Zeming Lin, Natalia Gimelshein, Luca Antiga, et al. Pytorch: An imperative style, high-performance deep learning library. *Advances in neural information processing systems*, 32, 2019.

William Peebles and Saining Xie. Scalable diffusion models with transformers. *arXiv preprint arXiv:2212.09748*, 2022.

Dustin Podell, Zion English, Kyle Lacey, Andreas Blattmann, Tim Dockhorn, Jonas Müller, Joe Penna, and Robin Rombach. Sdxl: Improving latent diffusion models for high-resolution image synthesis. *arXiv preprint arXiv:2307.01952*, 2023.

Adam Polyak, Amit Zohar, Andrew Brown, Andros Tjandra, Animesh Sinha, Ann Lee, Apoorv Vyas, Bowen Shi, Chih-Yao Ma, Ching-Yao Chuang, et al. Movie gen: A cast of media foundation models. *arXiv preprint arXiv:2410.13720*, 2024.

Alec Radford, Jeffrey Wu, Rewon Child, David Luan, Dario Amodei, Ilya Sutskever, et al. Language models are unsupervised multitask learners. *OpenAI blog*, 1(8):9, 2019.

Aditya Ramesh, Mikhail Pavlov, Gabriel Goh, Scott Gray, Chelsea Voss, Alec Radford, Mark Chen, and Ilya Sutskever. Zero-shot text-to-image generation. In *International conference on machine learning*, pp. 8821–8831. Pmlr, 2021.

Scott Reed, Konrad Zolna, Emilio Parisotto, Sergio Gomez Colmenarejo, Alexander Novikov, Gabriel Barth-Maron, Mai Gimenez, Yury Sulsky, Jackie Kay, Jost Tobias Springenberg, et al. A generalist agent. *arXiv preprint arXiv:2205.06175*, 2022.

Robin Rombach, Andreas Blattmann, Dominik Lorenz, Patrick Esser, and Björn Ommer. High-resolution image synthesis with latent diffusion models. In *Proceedings of the IEEE/CVF conference on computer vision and pattern recognition*, pp. 10684–10695, 2022.

Olaf Ronneberger, Philipp Fischer, and Thomas Brox. U-net: Convolutional networks for biomedical image segmentation. *ArXiv*, abs/1505.04597, 2015.

Olga Russakovsky, Jia Deng, Hao Su, Jonathan Krause, Sanjeev Satheesh, Sean Ma, Zhiheng Huang, Andrej Karpathy, Aditya Khosla, Michael Bernstein, et al. Imagenet large scale visual recognition challenge. *International journal of computer vision*, 115:211–252, 2015.

Subham Sahoo, Marianne Arriola, Yair Schiff, Aaron Gokaslan, Edgar Marroquin, Justin Chiu, Alexander Rush, and Volodymyr Kuleshov. Simple and effective masked diffusion language models. *Advances in Neural Information Processing Systems*, 37:130136–130184, 2024.

Tim Salimans, Ian Goodfellow, Wojciech Zaremba, Vicki Cheung, Alec Radford, and Xi Chen. Improved techniques for training gans. *Advances in neural information processing systems*, 29, 2016.

John Schulman, Filip Wolski, Prafulla Dhariwal, Alec Radford, and Oleg Klimov. Proximal policy optimization algorithms. *arXiv preprint arXiv:1707.06347*, 2017.

Jiaxin Shi, Kehang Han, Zhe Wang, Arnaud Doucet, and Michalis Titsias. Simplified and generalized masked diffusion for discrete data. *Advances in neural information processing systems*, 37:103131–103167, 2024.

Jiaming Song, Chenlin Meng, and Stefano Ermon. Denoising diffusion implicit models. *arXiv preprint arXiv:2010.02502*, 2020a.

Yang Song, Jascha Sohl-Dickstein, Diederik P Kingma, Abhishek Kumar, Stefano Ermon, and Ben Poole. Score-based generative modeling through stochastic differential equations. *arXiv preprint arXiv:2011.13456*, 2020b.

Khurram Soomro, Amir Zamir, and Mubarak Shah. Ucf101: A dataset of 101 human actions classes from videos in the wild. *ArXiv*, abs/1212.0402, 2012. URL https://api.semanticscholar.org/CorpusID:7197134.

Jianlin Su, Murtadha Ahmed, Yu Lu, Shengfeng Pan, Wen Bo, and Yunfeng Liu. Roformer: Enhanced transformer with rotary position embedding. *Neurocomputing*, 568:127063, 2024.

Peize Sun, Yi Jiang, Shoufa Chen, Shilong Zhang, Bingyue Peng, Ping Luo, and Zehuan Yuan. Autoregressive model beats diffusion: Llama for scalable image generation. *arXiv preprint arXiv:2406.06525*, 2024.

Chameleon Team. Chameleon: Mixed-modal early-fusion foundation models. *arXiv preprint arXiv:2405.09818*, 2024.

Keyu Tian, Yi Jiang, Zehuan Yuan, Bingyue Peng, and Liwei Wang. Visual autoregressive modeling: Scalable image generation via next-scale prediction. *arXiv preprint arXiv:2404.02905*, 2024.

Hugo Touvron, Thibaut Lavril, Gautier Izacard, Xavier Martinet, Marie-Anne Lachaux, Timothée Lacroix, Baptiste Rozière, Naman Goyal, Eric Hambro, Faisal Azhar, et al. Llama: Open and efficient foundation language models. *arXiv preprint arXiv:2302.13971*, 2023a.

Hugo Touvron, Louis Martin, Kevin Stone, Peter Albert, Amjad Almahairi, Yasmine Babaei, Nikolay Bashlykov, Soumya Batra, Prajjwal Bhargava, Shruti Bhosale, et al. Llama 2: Open foundation and fine-tuned chat models. *arXiv preprint arXiv:2307.09288*, 2023b.

Aaron Van Den Oord, Oriol Vinyals, et al. Neural discrete representation learning. *Advances in neural information processing systems*, 30, 2017.

Ashish Vaswani, Noam Shazeer, Niki Parmar, Jakob Uszkoreit, Llion Jones, Aidan N Gomez, Łukasz Kaiser, and Illia Polosukhin. Attention is all you need. *NeurIPS*, 30, 2017.

Junke Wang, Yi Jiang, Zehuan Yuan, Binyue Peng, Zuxuan Wu, and Yu-Gang Jiang. Omnitokenizer: A joint image-video tokenizer for visual generation. *arXiv preprint arXiv:2406.09399*, 2024a.

Xinlong Wang, Xiaosong Zhang, Zhengxiong Luo, Quan Sun, Yufeng Cui, Jinsheng Wang, Fan Zhang, Yueze Wang, Zhen Li, Qiying Yu, et al. Emu3: Next-token prediction is all you need. *arXiv preprint arXiv:2409.18869*, 2024b.

Mark Weber, Lijun Yu, Qihang Yu, Xueqing Deng, Xiaohui Shen, Daniel Cremers, and Liang-Chieh Chen. Maskbit: Embedding-free image generation via bit tokens. *arXiv preprint arXiv:2409.16211*, 2024.

Jialong Wu, Shaofeng Yin, Ningya Feng, Xu He, Dong Li, Jianye Hao, and Mingsheng Long. ivideogpt: Interactive videogpts are scalable world models, 2024a.

Yecheng Wu, Zhuoyang Zhang, Junyu Chen, Haotian Tang, Dacheng Li, Yunhao Fang, Ligeng Zhu, Enze Xie, Hongxu Yin, Li Yi, et al. Vila-u: a unified foundation model integrating visual understanding and generation. *arXiv preprint arXiv:2409.04429*, 2024b.

Jinheng Xie, Weijia Mao, Zechen Bai, David Junhao Zhang, Weihao Wang, Kevin Qinghong Lin, Yuchao Gu, Zhijie Chen, Zhenheng Yang, and Mike Zheng Shou. Show-o: One single transformer to unify multimodal understanding and generation. *arXiv preprint arXiv:2408.12528*, 2024.

An Yang, Baosong Yang, Binyuan Hui, Bo Zheng, Bowen Yu, Chang Zhou, Chengpeng Li, Chengyuan Li, Dayiheng Liu, Fei Huang, et al. Qwen2 technical report. *arXiv preprint arXiv:2407.10671*, 2024.

Mengjiao Yang, Yilun Du, Kamyar Ghasemipour, Jonathan Tompson, Dale Schuurmans, and Pieter Abbeel. Learning interactive real-world simulators. *arXiv preprint arXiv:2310.06114*, 2023.

Ziyu Yao, Jialin Li, Yifeng Zhou, Yong Liu, Xi Jiang, Chengjie Wang, Feng Zheng, Yuexian Zou, and Lei Li. Car: Controllable autoregressive modeling for visual generation. *arXiv preprint arXiv:2410.04671*, 2024.

Jiahui Yu, Yuanzhong Xu, Jing Yu Koh, Thang Luong, Gunjan Baid, Zirui Wang, Vijay Vasudevan, Alexander Ku, Yinfei Yang, Burcu Karagol Ayan, et al. Scaling autoregressive models for content-rich text-to-image generation. *arXiv preprint arXiv:2206.10789*, 2(3):5, 2022.

Lijun Yu, Yong Cheng, Kihyuk Sohn, José Lezama, Han Zhang, Huiwen Chang, Alexander G Hauptmann, Ming-Hsuan Yang, Yuan Hao, Irfan Essa, et al. Magvit: Masked generative video transformer. In *Proceedings of the IEEE/CVF Conference on Computer Vision and Pattern Recognition*, pp. 10459–10469, 2023a.

Lijun Yu, José Lezama, Nitesh B Gundavarapu, Luca Versari, Kihyuk Sohn, David Minnen, Yong Cheng, Agrim Gupta, Xiuye Gu, Alexander G Hauptmann, et al. Language model beats diffusion–tokenizer is key to visual generation. *arXiv preprint arXiv:2310.05737*, 2023b.

Chuyang Zhao, Yuxing Song, Wenhao Wang, Haocheng Feng, Errui Ding, Yifan Sun, Xinyan Xiao, and Jingdong Wang. Monoformer: One transformer for both diffusion and autoregression. *arXiv preprint arXiv:2409.16280*, 2024a.

Haoyu Zhao, Tianyi Lu, Jiaxi Gu, Xing Zhang, Qingping Zheng, Zuxuan Wu, Hang Xu, and Yu-Gang Jiang. Magdiff: Multi-alignment diffusion for high-fidelity video generation and editing. In *European Conference on Computer Vision*, pp. 205–221. Springer, 2024b.

Chunting Zhou, Lili Yu, Arun Babu, Kushal Tirumala, Michihiro Yasunaga, Leonid Shamis, Jacob Kahn, Xuezhe Ma, Luke Zettlemoyer, and Omer Levy. Transfusion: Predict the next token and diffuse images with one multi-modal model. *arXiv preprint arXiv:2408.11039*, 2024a.

Siyuan Zhou, Yilun Du, Jiaben Chen, Yandong Li, Dit-Yan Yeung, and Chuang Gan. Robodreamer: Learning compositional world models for robot imagination. *arXiv preprint arXiv:2404.12377*, 2024b.

A Detailed Discussion about Block Size

In this section, we provide a detailed analysis of the computational cost of ACDiT in terms of FLOPS, comparing it to standard full-sequence diffusion in transformer layers. Let L denote the sequence length, h the hidden size, n the number of attention heads (assumed $n \ll h$), θ the number of parameters in a single transformer layer, and B the block size used in ACDiT.

Full-Sequence FLOPS. Each transformer layer has two major computational components:

- Linear projections and feed-forward layers: $2L\theta$
- Q–K attention dot-products: $4(h+n)L^2 \approx 4hL^2$

Hence, the total FLOPS per layer is:

$$F_{\text{full}} = 2L\theta + 4hL^2$$

ACDiT with KV-Cache. In ACDiT, attention is computed block-wise using KV-Cache. The i-th block (of size B) attends to $(i-1)B$ cached tokens, requiring iB^2 Q–K dot-products. Summing over all $\frac{L}{B}$ blocks:

$$\sum_{i=1}^{L/B} iB^2 = B^2 \cdot \frac{L}{B} \cdot \left(\frac{L}{B} + 1\right) \Big/ 2 = \frac{L^2 + LB}{2}$$

So the attention FLOPS becomes:

$$\text{Attention}_{\text{ACDiT}} = 4h \cdot \frac{L^2 + LB}{2} = 2hL^2 + 2hLB$$

Including projection and FFN cost, the total FLOPS under ACDiT is:

$$F_{\text{ACDiT}} = 2L\theta + 2hL^2 + 2hLB$$

FLOPS Savings. The absolute FLOPS saved per layer is:

$$F_{\text{saved}} = F_{\text{full}} - F_{\text{ACDiT}} = 2hL^2(1 - \tfrac{B}{L})$$

The relative savings are:

$$\frac{F_{\text{saved}}}{F_{\text{full}}} = \frac{2hL^2(1 - \frac{B}{L})}{2L\theta + 4hL^2} = \frac{1 - \frac{B}{L}}{2 + \frac{\theta}{hL}}$$

When $L \gg h$, the savings approaches $\frac{1}{2}(1 - \frac{B}{L})$, implying up to 50% FLOPS reduction when $B \ll L$.

In practice, it is not always beneficial for small B. Setting B to an excessively small value may not fully leverage the iterative modification inherent in the diffusion process, potentially compromising generation quality. Furthermore, given the parallel computing nature of computational kernels, a very small B may not yield speed improvements, a phenomenon analogous to the rationale behind speculative decoding (Leviathan et al., 2023). Conversely, setting B to a very large value diminishes efficiency both in terms of attention calculation. It also fails to capitalize on the strengths of auto-regressive generation. Indeed, when B is set equal to L, ACDiT reverts to the original DiT model.

B Details of Model Architecture and Implementation

ACDiT mainly inherits the main architecture of DiT. We replace the original bidirectional attention with the proposed SCAM attention pattern to process the clean and noisy latent. Since we want to keep the architecture as simple and unified as possible, we use linear layers instead of convolution in the input layer and final layer. Besides, we replace the position embedding and Layer Normalization with RoPE (Su et al.,

Table 5: Configuration details of ACDiT.

Model	#Layers	Hidden Size	MLP	#Heads	Params
ACDiT-B	12	768	3072	12	132M
ACDiT-L	24	1024	4096	16	460M
ACDiT-XL	28	1152	4608	18	677M
ACDiT-H	32	1280	5120	20	954M

2024) and RMSNorm (Root Mean Square Layer Normalization) (Touvron et al., 2023a), respectively. We find that QK-norm is important to stabilizing the video generation training, thus we use QK-norms in all experiments. The additional conditional information, including timesteps and labels, is injected into the model with AdaLN-Zero only on the noise part. For both image and video generation, we follow DiT and leverage the pre-trained image VAE (Kingma, 2013) from Stable Diffusion (Rombach et al., 2022), whose downsample factor is 8. For image generation under B block size, we group square latent representation patches with $\sqrt{B} \times \sqrt{B}$ shape as a block. We do not further train the tokenizer in the target dataset since it's out of the scope of our work, despite that further training might yield better results.

In the image generation task, we set the patch size as 1 and the autoregressive unit block size as $256 = 16 \times 16$. Therefore, for a $256 \times 256 \times 3$ image in $32 \times 32 \times 4$ latent shape, the total sequence length and autoregressive length are 1024 and 4, respectively. We explore 4 different model sizes, as shown in Table 5. ACDiT-B is used for design verification and analysis. ACDiT is trained on ImageNet for 1.2M iterations with a batch size of 1024. We use the AdamW optimizer (Loshchilov, 2017) and WSD (Warmup Steady Decay) learning rate scheduling (Hu et al., 2024) with the peak learning rate 3e-4 and no weight decay. The learning rate begins to decay in the last 15% training iterations. Following the common training recipe of generative models, we keep an exponential moving average (EMA) of the ACDiT weights during training using a decay rate of 0.9999. We sample images with DPM-Solver (Lu et al., 2022) for 25 steps within each block and use classifier-free guidance (Ho & Salimans, 2022) with a guidance scale of 1.5. In video generation, we sample 16 frames from each video and set the patch size as 2 and the block size as $1024 = 256 \times 4$. For a $16 \times 256 \times 256 \times 3$ video in $16 \times 32 \times 32 \times 4$ latent shape, the sequence length of each frame is 256 and the total sequence length is 4096, with 4 frames grouped into one block. We train ACDiT on UCF-101 for 400K iterations with a batch size of 96. The classifier-free guidance scale is 2.5. Other training configs are the same as image training. All models are implemented with PyTorch (Paszke et al., 2019). Specifically, we use FlexAttention[3] to implement the SCAM for both customization and efficiency. We use 256 and 96 NVIDIA H100 GPUs to train the image and video generation model, respectively.

C Qualitative Results of ACDiT

We show the qualitative results of ACDiT in Figure 7.

[3]https://pytorch.org/blog/flexattention

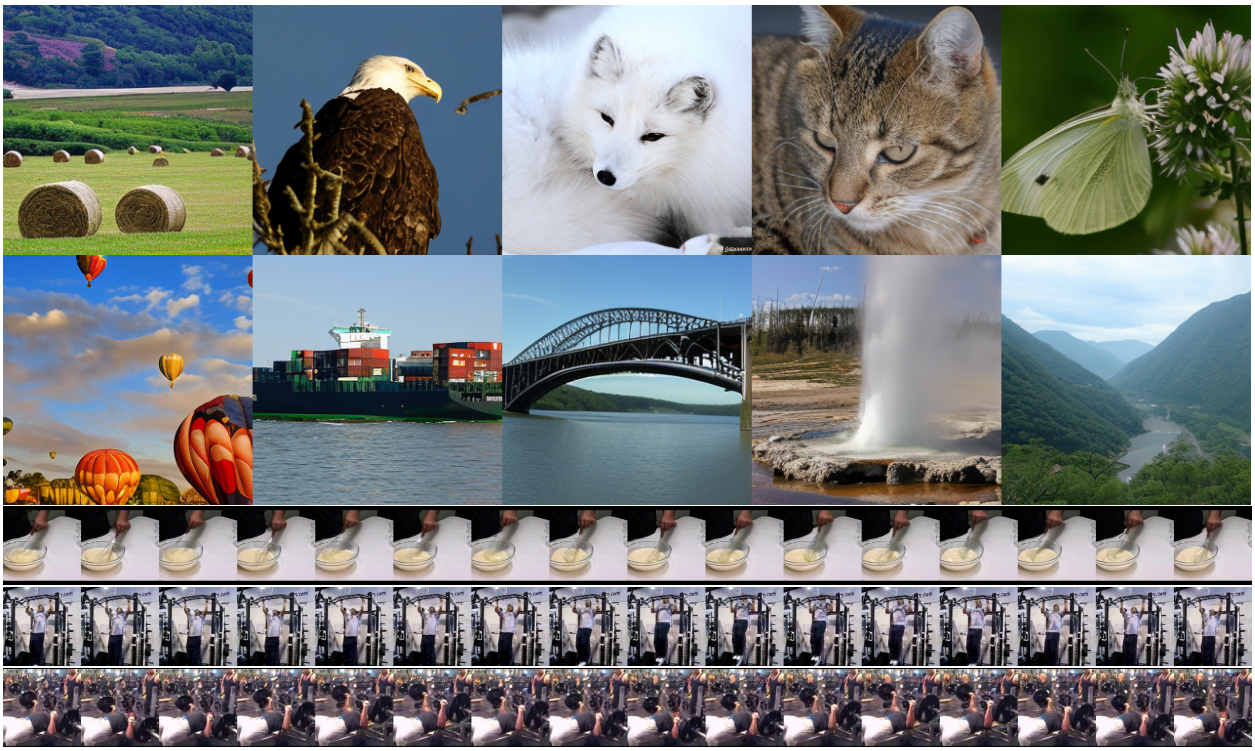

Figure 7: Sample images from ACDiT-H on ImageNet 256×256 and sample videos from ACDiT-XL trained on UCF-101.